APL Materials

RESEARCH ARTICLE | APRIL 04 2025

Magnetic phase diagram of $Mn_{3+x}Sn_{1-x}$ epitaxial thin films: Extending the anomalous Hall effect to low temperatures via intrinsic alloying

Special Collection: Energy-Efficient Memory Materials

K. Gas ; J.-Y. Yoon ; Y. Sato ; H. Kubota ; P. Dłużewski ; S. Kret ; J. Z. Domagala ; Y. K. Edathumkandy ; Y. Takeuchi ; S. Kanai ; H. Ohno ; M. Sawicki ; S. Fukami

APL Mater. 13, 041105 (2025)
https://doi.org/10.1063/5.0254918

Magnetic phase diagram of $Mn_{3+x}Sn_{1-x}$ epitaxial thin films: Extending the anomalous Hall effect to low temperatures via intrinsic alloying

Cite as: APL Mater. 13, 041105 (2025); doi: 10.1063/5.0254918
Submitted: 25 December 2024 • Accepted: 15 March 2025 •
Published Online: 4 April 2025

K. Gas,[1,2,a] J.-Y. Yoon,[3,4] Y. Sato,[3,4] H. Kubota,[3,4] P. Dłużewski,[2] S. Kret,[2] J. Z. Domagala,[2] Y. K. Edathumkandy,[2] Y. Takeuchi,[3,5,6] S. Kanai,[1,3,4,6,7,8,9] H. Ohno,[1,3,7,10] M. Sawicki,[2,3,a] and S. Fukami[1,3,4,7,10,11,a]

AFFILIATIONS

[1]Center for Science and Innovation in Spintronics, Tohoku University, 2-1-1 Katahira, Aoba-ku, Sendai 980-8577, Japan
[2]Institute of Physics, Polish Academy of Sciences, Aleja Lotnikow 32/46, PL-02668 Warsaw, Poland
[3]Laboratory for Nanoelectronics and Spintronics, Research Institute of Electrical Communication, Tohoku University, 2-1-1 Katahira, Aoba-ku, Sendai 980-8577, Japan
[4]Graduate School of Engineering, Tohoku University, 6-6 Aoba, Aramaki, Aoba-ku, Sendai 980-8579, Japan
[5]International Center for Young Scientists (ICYS), National Institute for Materials Science (NIMS), 1-2-1 Sengen, Tsukuba, Ibaraki 305-0047, Japan
[6]PRESTO, Japan Science and Technology Agency (JST), Kawaguchi, Japan
[7]Advanced Institute for Materials Research, Tohoku University, 2-1-1 Katahira, Aoba-ku, Sendai 980-8577, Japan
[8]DEFS, Tohoku University, Katahira 2-1-1, Aoba-ku, Sendai 980-8577, Japan
[9]National Institutes for Quantum Science and Technology, Takasaki, Japan
[10]Center for Innovative Integrated Electronic Systems, Tohoku University, 468-1 Aoba, Aramaki, Aoba-ku, Sendai 980-8572, Japan
[11]Inamori Research Institute for Science, Kyoto 600-8411, Japan

Note: This paper is part of the Joint Special Topic on Energy-Efficient Memory Materials from APL Materials and APL Energy.
[a]**Authors to whom correspondence should be addressed:** gas.katarzyna.a2@tohoku.ac.jp; mikes@ifpan.edu.pl; and s-fukami@riec.tohoku.ac.jp

ABSTRACT

Antiferromagnets with broken time-reversal symmetry, such as Mn_3Sn, have emerged as promising platforms for exploring topological and correlated electron physics. Mn_3Sn is known to show two magnetic phase transitions: a non-collinear inverse triangular antiferromagnetic (IT-AFM) spin configuration is formed below its Néel temperature ($T_N \cong 420$ K), whereas at T_1 that usually locates below room temperature, it transits to an incommensurate spin state. Accordingly, intriguing properties such as a strong anomalous Hall effect, observed from T_N to T_1, disappear below T_1, limiting its utility at low temperatures. While bulk Mn_3Sn has been extensively studied, the magnetic phase transitions and their tunability in thin films remain largely unexplored. Here, we investigate the magnetic and magneto-transport properties of $Mn_{3+x}Sn_{1-x}$ epitaxial thin films prepared by magnetron sputtering, systematically varying the Mn–Sn composition. Our results reveal that intrinsic alloying with Mn provides us with a handle to tune T_1, with the IT-AFM phase stabilized down to liquid helium temperatures for $x > 0.15$. From a magnetic phase diagram for epitaxial thin films, we also find a consistent magnetic anomaly ~55 K below T_N, accompanied by thermal hysteresis. Furthermore, the reduction in T_N in thin films relative to bulk values is shown to correlate with lattice parameter changes. These findings extend the accessible temperature range for Mn_3Sn's topological properties, paving the way for novel applications and further investigations into the interplay of spin, lattice, and electronic degrees of freedom in thin-film geometries.

I. INTRODUCTION

Antiferromagnets with macroscopically broken time-reversal symmetry emerge as promising materials for spintronics due to their unique properties, which overcome some of the limitations of ferromagnetic materials.[1–6] Mn_3Sn is a representative system in antiferromagnetic (AFM) spintronics. It crystallizes in a hexagonal $D0_{19}$ structure belonging to the space group $P6_3/mmc$. Below its Néel temperature ($T_N \cong 420$ K), Mn_3Sn adopts a non-collinear inverse triangular antiferromagnetic (IT-AFM) spin configuration within its kagome lattice, with spins forming 120° angles and a negative vector chirality in the basal a–b plane (0001).[7–9] The magnetic structure of Mn_3Sn is characterized by the ferroic ordering of cluster magnetic octupoles, which serves as the key order parameter breaking time-reversal symmetry.[10,11] This symmetry breaking leads to the emergence of significant Berry curvature in momentum space, particularly near Weyl points.[12,13] Consequently, despite its negligible net magnetization, Mn_3Sn displays substantial non-trivial transport phenomena, including a large anomalous Hall effect (AHE),[1] the anomalous Nernst effect,[14] the second-order Hall effect,[15] and the tunneling magnetoresistance effect,[16] all originating from its unique band structure, highlighting its potential for spintronic applications. Furthermore, the slight canting of Mn moments within the (0001) plane produces a small ferromagnetic moment (~0.002 μ_B/Mn, where μ_B is the Bohr magneton),[8,17] allowing external magnetic fields to control the antiferromagnetic order. This distinctive combination of magnetic and transport properties offers immense potential for the electrical manipulation of the AFM order, analogous to that observed in ferromagnets.[18–20]

For the investigation of the functionalities of non-collinear antiferromagnets, an in-depth understanding of their magnetic phase transitions is of high importance. In the case of Mn_3Sn, the Néel temperature (T_N) is a critical parameter, particularly in the context of Joule heating, as it defines the operational temperature range of the material.[21] Surface effects alone can reduce the already relatively low T_N of Mn_3Sn crystals by as much as 10 K,[22] highlighting the need to explore the factors influencing T_N in different material configurations. Below room temperature, some of the Mn_3Sn crystals undergoes a magnetic phase transition at T_1 (which can be as close to room temperature as 275 K) from the IT-AFM spin configuration to an incommensurate magnetic phase.[9,23] The exact spin structure of the incommensurate phase remains an active area of research. This low-temperature spin state was previously thought to be a heterogeneous blend of two helical magnetic phases.[9,24] However, very recent studies demonstrated that it is a homogeneous incommensurate spin and charge-modulated phase, characterized by two fundamental wave vectors that transition continuously from incommensurate to commensurate as the temperature decreases.[23] The transition from the IT-AFM spin configuration to an incommensurate magnetic phase is not only significant for understanding low-temperature physics but also significant for its impact on properties such as AHE and weak magnetization, of which both are suppressed below T_1.[25] Meanwhile, for Mn_3Sn crystals, which do not exhibit a transition to the incommensurate spin state, a spin-glass like behavior was observed, and no large AHE characteristic to the inverse triangular spin configuration was reported.[1,8,17] The T_1 transition is also attracting attention due to its origin based on charge and spin density-wave instabilities associated with the Fermi-surface nesting[26] of flatbands.[23] This nesting phenomenon is highly sensitive to variations in the chemical potential and the bond lengths between Mn atoms, which jointly influence the band structure and may explain the sample-dependent incommensurability observed in Mn_3Sn.[1,9,25,27–29] While the knowledge of the nature of the T_1 transition continues to grow,[23,29] the precise material parameters governing its mechanisms still need to be investigated for a comprehensive understanding of this phenomenon. Density functional theory calculations suggest that the Fermi energy E_F is strongly influenced by the amount of excess Mn content, with E_F increasing by ~6 meV for each percent of substitutional Mn atoms.[12] These effects provide valuable insights into the interplay between topology and electron correlations and even open pathways for exploring novel topological phases in magnetic materials. However, the suppression of the AHE below T_1 limits Mn_3Sn's utility in investigating the low-temperature physics of octupolar order.[30]

While magnetic phase transitions such as T_N and T_1 have been reasonably well studied in bulk Mn_3Sn,[27] their behavior and tunability in thin-film structures are not well understood. Thin films often exhibit significant differences in transition temperatures compared to their bulk counterparts due to structural factors such as surface effects, epitaxial strain, and the presence of heterogeneous substrate and seed layers. Despite the importance of T_N as a material parameter, its study has not been a primary focus in thin-film research thus far. Although experimental investigations face significant challenges—particularly the difficulty of detecting tiny magnetizations in AFM materials—studies of these phase transitions in thin films are essential for a complete understanding of their magnetic and electronic properties and an exploration of device functionalities.

It is, therefore, timely and important to systematically study the magnetic transition temperatures in thin films of Mn_3Sn with a varying Mn–Sn composition. This will facilitate the identification of the conditions that result in the formation of the magnetic phase showing intriguing device functionalities, i.e., the IT-AFM spin configuration. In addition, it will enable the study of novel physics in strongly correlated systems that usually arise at lower temperatures. To this end, we investigate the temperature dependence of magnetic and magneto-transport properties of $Mn_{3+x}Sn_{1-x}$ thin films, prepared by intrinsic alloying understood as the incorporation of excess Mn atoms into the Mn_3Sn lattice. This self-regulating adjustment of the Mn–Sn ratio inherently tailors the material's composition and properties without the need for external dopants. We establish precise values of the magnetic transition temperatures, showing that for $x > 0.15$, the inverse triangular spin configuration, which hosts the strong AHE, can be stabilized down to the liquid helium temperature. Our results are summarized into the magnetic phase diagram for $Mn_{3+x}Sn_{1-x}$ epitaxial thin films, in which a magnetic anomaly below the paramagnetic–antiferromagnetic transition has been identified. We also highlight a clear correlation between T_N reduction and lattice parameter changes induced by composition in thin films.

II. SAMPLES AND METHODS

$Mn_{3+x}Sn_{1-x}$ layers are deposited on single crystal MgO(110) substrates by DC/RF magnetron sputtering according to previously elaborated protocols.[31] The sample stacks, depicted in Fig. 1(a),

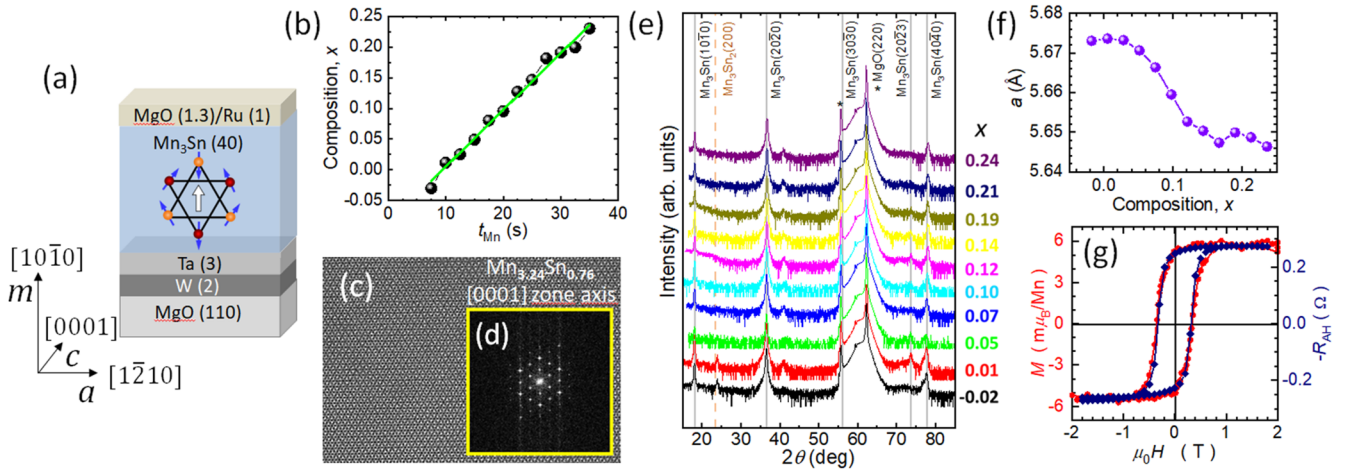

FIG. 1. Sample layout and structural properties of $Mn_{3+x}Sn_{1-x}$ films. (a) Schematic of the sample stack with thicknesses (in nm) of the constituent layers indicated in the parentheses. The inverse triangular spin arrangement in Mn_3Sn is depicted in the central part. The red and orange spheres represent Mn atoms in two consecutive kagome planes. The blue arrows represent the magnetic moments of Mn atoms. The cluster magnetic octupole is represented by the white arrow. The coordinate system defines the crystallographic relations of Mn_3Sn. (b) (Black bullets) Exceeding Mn composition, x, as a function of Mn single target sputtering time t_{Mn}. The green line represents the linear fit to the data. (c) Transmission electron microscope image in the [0001] zone axis of the $Mn_{3.24}Sn_{0.76}$ film. (d) 2D diffraction pattern taken from a central fragment of (c). (e) $2\theta/\omega$ diffraction patterns of the samples (offset for clarity). (f) a lattice parameter dependence on x. (g) Comparison of magnetization, M (red circles), and anomalous Hall resistance, R_{AH} (navy diamonds), magnetic field H loops ($H \| [10\bar{1}0]$) for the $Mn_{3.07}Sn_{0.93}$ film at T = 300 K. A linear increase in $M(H)$ due to spin canting has been additionally compensated. Note the inverse polarity of $R_{AH}(H)$ loop with respect to $M(H)$.

consist of, from the substrate side, a W (2 nm)/Ta (3 nm) seed layer followed by 40 nm of $Mn_{3+x}Sn_{1-x}$ and terminated by a MgO (1.3 nm)/Ru (1 nm) cap. W, Ta, $Mn_{3+x}Sn_{1-x}$, and Ru are deposited at 400 °C, and MgO is deposited at room temperature. All steps are done under a base pressure of less than 1×10^{-6} Pa. The established stack structure allows for obtaining $(10\bar{1}0)$-oriented (m-plane in the hexagonal short-hand notation) epitaxial $Mn_{3+x}Sn_{1-x}$ films with the kagome plane perpendicular to the film plane.[31–33] The deviation x from the stoichiometric composition in the $Mn_{3+x}Sn_{1-x}$ series is set by alternating 50 s of Mn–Sn co-sputtering and t_{Mn} (7.5–35.0 s) of Mn single-target sputtering.[34,35] The consequent Mn–Sn composition is determined by inductively coupled plasma mass spectrometry. We adopt the $Mn_{3+x}Sn_{1-x}$ notation following Refs. 34 and 35. The resulting magnitudes of x show a monotonic increase with t_{Mn}, as displayed in Fig. 1(b), and can be approximated by a linear function.

The homogeneous $D0_{19}$ structure of Mn_3Sn is obtained through post-deposition annealing at vacuum by heating the samples to 600 °C at a rate of 10 °C/min, holding for 90 min at the target temperature, and subsequent cooling to room temperature. The material is typically divided into 5×5 or 10×5 mm^2 specimens. The former is used for magnetic and/or electrical measurements in the van der Pauw configuration, whereas the latter is used for the electrical measurements with lithographically processed double-bridge-type Hall bar structures. Magnetic and electrical measurements in a wide temperature T range from 5 to 400 K are performed in the perpendicular orientation of magnetic field H ($H \| [10\bar{1}0]$) using Quantum Design's superconducting quantum interference device (SQUID) magnetometer MPMS XL5 and Physical Property Measuring Systems (PPMS), respectively. We strictly follow the experimental code of sensitive magnetometry.[36,37] DC electrical excitation is used for electrical studies. The Titan Cubed 80-300 transmission electron microscope (TEM) operating with an accelerating voltage of 300 kV is used for this study. The crystal structure and lattice parameters are determined using an x-ray diffractometer with a wavelength of 1.5406 Å of the Cu $K_{\alpha 1}$ line.

III. RESULTS AND DISCUSSION

A. Structural, magnetic, and magneto-transport characterizations at room temperature

The cross-sectional TEM images shown in Fig. 1(c) and a corresponding electron diffraction pattern [Fig. 1(d)] for a stack with x = 0.24 corroborate the synthesis of high-quality epitaxial films of the m-plane $D0_{19}$-$Mn_{3+x}Sn_{1-x}$ even with a high Mn content. X-ray diffraction patterns for all the specimens in this study are shown in Fig. 1(e). The positions of the $20\bar{2}0$ reflections allow us to trace the evolution of the a lattice parameter with x [shown in Fig. 1(f)]. Our findings confirm that a generally decreases with x, aligning with the dependency previously established for epitaxial thin films[34] and bulk polycrystalline samples.[27] The decrease in a implies the substitutional Mn incorporation into the Sn site, rather than assuming interstitial positions. This is consistent with the fact that Mn has a smaller atomic radius than Sn, leading to a basal plane contraction when Mn replaces Sn. If Mn occupied interstitial positions, we would expect the lattice parameter to expand due to lattice distortion effects, contrary to our data presented in Fig. 1 (f). However, the flattening of the $a(x)$ dependency seen above x = 0.15 indicates that not all Mn atoms provided during intrinsic alloying are substitutionally incorporated into the lattice. This suggests that a thermodynamic limit for Mn incorporation may have been reached.[27] It is supported

by the observation of sub-micrometer-sized Mn-rich deposits on the surface of these films (shown in Fig. S1 of the supplementary material). Since the as-deposited material crystallizes during high-temperature annealing,[34] it is most likely that these deposits form at this stage rather than during deposition. For near stoichiometric layers, additional diffraction peaks from $B8$-Mn_3Sn_2 are also observed, consistent with previous study.[35]

We then measure the magnetization (M) and the anomalous Hall resistance (R_{AH}). A typical example for the $Mn_{3.07}Sn_{0.93}$ film at T = 300 K is shown in Fig. 1(g). A strong magnetic contribution from the MgO substrate[38] and a linear increase in $M(H)$ due to spin canting have been removed. A good consistency in response to the applied magnetic field is confirmed. We highlight two challenges here. The first is that the diamagnetic signal from a typical $5 \times 5 \times 0.5$ cm^3 MgO substrate dwarfs that of the AFM layers in question, as shown in Fig. S2 of the supplementary material. Namely, above 10^{-4} emu and below 5×10^{-6} emu at $\mu_0 H$ = 1 T, respectively (μ_0 is the permeability of vacuum). Moreover, the latter decreases by another order of magnitude as T approaches T_N. Second, the presence of a relatively strong soft ferromagnetic-like component in the MgO substrates alone "dissects" the square-like hysteresis loop of Mn_3Sn, leading to false double switching behavior and saturation levels. Overcoming these experimental hurdles proved to be essential in order to determine all the details of the magnetic phase diagram reported in this study. Our experimental approach is outlined in Sec. S II of the supplementary material (Refs. 39–42). A clear relationship between M and R_{AH} further supports the general understanding that the applied magnetic field couples with a small, uncompensated weak ferromagnetic-like moment (WFM), which forms within the hexagonal crystal planes. Meanwhile, results in Fig. 1(g) indicate that our Mn_3Sn layers exhibit spontaneous magnetization magnitudes (about 2.5 mT or 20 mμ_B per formula unit at 300 K) approximately three times larger than those of bulk samples.[1,43] This enhanced magnetization is likely due to the tensile epitaxial strain, which was shown to significantly affect the magnitude of WFM.[44]

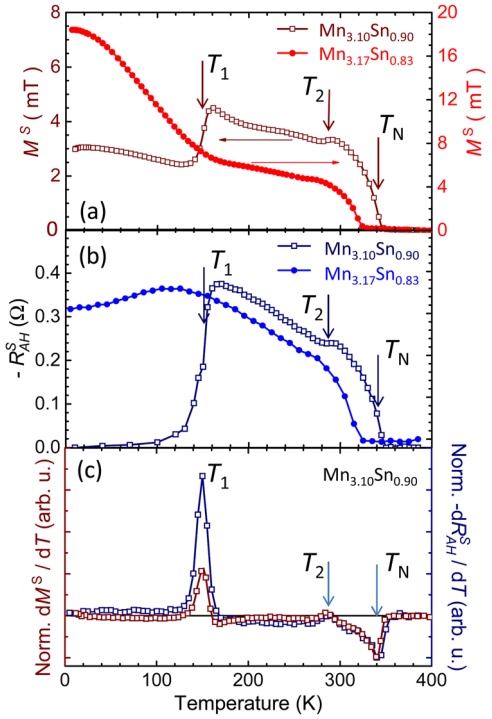

FIG. 2. (a) and (b) Temperature dependence of the spontaneous magnetization, $M^S(T)$, and anomalous Hall resistance, $R^S_{AH}(T)$, respectively, recorded on cooling in an external magnetic field $\mu_0 H_{FC}$ = 10 mT for $Mn_{3.10}Sn_{0.90}$ (open squares) and $Mn_{3.17}Sn_{0.83}$ (bullets). (c) Temperature derivatives $dM^S(T)/dT$ and $dR^S_{AH}(T)/dT$ from (a) and (b) for $Mn_{3.10}Sn_{0.90}$. The positions of the Néel, T_N, and T_1 transitions, and an anomaly, which we mark as T_2, are indicated by the arrows for the $Mn_{3.10}Sn_{0.90}$ only (for clarity). The T_2 anomaly is discussed in Sec. III D.

B. Temperature dependent magnetization and magneto-transport measurements

The information extracted from the temperature dependences of the spontaneous magnetization $M^S(T)$ and spontaneous anomalous Hall resistance $R^S_{AH}(T)$ provides us with an overview of the magnetic properties of $Mn_{3+x}Sn_{1-x}$ films in the wide temperature range. Figures 2(a) and 2(b) show the results obtained from two representative films, with x = 0.10 and 0.17. Both $M^S(T)$ and $R^S_{AH}(T)$ are measured by cooling from 400 K in a weak magnetic field $\mu_0 H_{FC}$ = 10 mT. The first clear feature is that the AFM Néel transition takes place below 400 K in both films. It is noteworthy that the Néel transition in Mn_3Sn is evidenced by a positive surge in magnetization. This ferromagnetic-like behavior arises from the combined effects of the formation of small WFMs and their unimpeded ordering along nonzero $\mu_0 H_{FC}$ at $T \cong T_N$. This simultaneously orders the octupole moments, resulting in an equally abrupt emergence of R^S_{AH}.

The second important feature is the profound qualitative difference seen between these samples at low temperatures, starting below 170 K. We observe that whereas the x = 0.10 sample undergoes the T_1 transition from the inverse triangular antiferromagnetic to an incommensurate spin configuration[23] at about T_1 = 150 K, this transition is absent in the x = 0.17 film. Subsequently, the strong AHE signal characteristic for Mn_3Sn is preserved down to the lowest temperatures in $Mn_{3.17}Sn_{0.83}$.

The sole weak temperature dependence of R^s_{AH} for $Mn_{3.17}Sn_{0.83}$ down to 5 K [Fig. 2(b)] unequivocally demonstrates that the same negative polarity and substantial values of AHE remain unaltered until the lowest temperatures. To further substantiate this finding, we present in Figs. 3(a) and 3(b) the temperature evolution of AHE loops, $R_{AH}(H)$, for the same two samples considered in Figs. 2(a) and 2(b). The correlation with the T-dependent data of Fig. 2 is indisputable. That is, for $Mn_{3.10}Sn_{0.90}$, the T_1 transition is observed, resulting in the disappearance of AHE at low temperatures, whereas for $Mn_{3.17}Sn_{0.83}$, it is absent, leading to a strong AHE in the whole temperature range down to 5 K.

The summary of the AHE results for the full x range of studied samples, taken at 300 and 5 K as the representative temperatures, is presented in Fig. 3(c). First, we note that the magnetic octupole hosting the $D0_{19}$-Mn_3Sn structure is realized for all compositions of Mn, including the below-stoichiometric one (see also Fig. S3 of the supplementary material). As previously reported,[35] the strongest AHE at room temperature occurs in moderately doped films ($x \cong 0.1$). Temperature-dependent measurements reveal that the

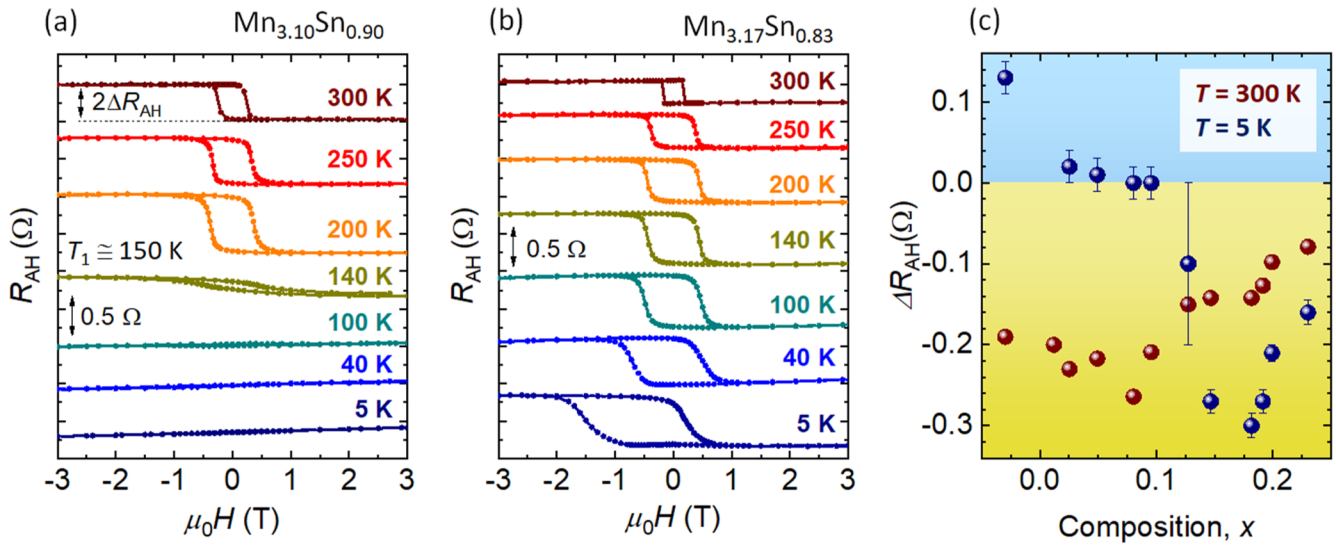

FIG. 3. (a) and (b) Temperature evolution of the anomalous Hall resistance R_{AH} in $Mn_{3+x}Sn_{1-x}$ films. The linear background of transverse resistance has been subtracted, and the results are shifted vertically for clarity. The measurements are performed on warming after cooling at $\mu_0 H_{FC}$ = 1 T. (c) Composition dependence of magnitudes of ΔR_{AH} [defined in (a)] established at 5 K (navy) and 300 K (brown). The sign of ΔR_{AH} represents the polarity of the AHE loop. The magnitude of the error bars is set by the residual curvature of $R_{AH}(H)$ at high magnetic fields.

AHE diminishes at low temperatures for these concentrations. It is either quenched completely or acquires FM-like polarity; the latter phenomenon may be attributed to the presence of additional magnetic phases.[25,34,45] In contrast, all films with $x \geq 0.15$ exhibit a robust AHE response persisting down to at least 5 K, with the same negative polarity indicative of its octupolar origin. The $Mn_{3.12}Sn_{0.88}$ film appears to be a borderline case worthy of further investigation.

The results in Fig. 3(b) also point out one more intriguing phenomenon. The low-T $R_{AH}(H)$, as well as $M(H)$ (not shown here), is biased in the opposite direction to the sign of H, in which the sample was initially cooled down, $\mu_0 H_{FC}$ = +1 T, thereby resembling the classical exchange bias effect.[46] This feature is observed in all the samples, in which the IT-AFM extends to the lowest temperatures. It is noteworthy that various biasing effects have been reported for bare Mn_3Sn even at room temperature.[47,48] In these cases, some kind of nanoscale phase coexistence was invoked to provide a firmly biased pinning component. However, no evidence supporting such possibilities has been found in our films. A more in-depth investigation of the origin of this low-T AHE shift is beyond the scope of this article.

We summarize this part by noting that the accumulated body of evidence presented in Figs. 1–3 decisively indicates that a significant substitution of Sn by Mn in Mn_3Sn leads to the stabilization of the IT-AFM phase down to the lowest temperatures without any particular detrimental effects to the structural constitution of this compound.

C. T_N dependence on x

We now consider the variation of T_N with x. The transition temperatures are determined from the positions of extrema in the $dM^S(T)/dT$ and $dR^S_{AH}(T)/dT$ derivatives; the representative results for $Mn_{3.10}Sn_{0.90}$ are shown in Fig. 2(c). We underline here that both derivatives indicate the same characteristic temperatures, meaning that the measurements of either $M^S(T)$ or $R^S_{AH}(T)$ provide with equally accurate magnitudes of T_N and T_1.

The dependence of T_N on x is shown in Fig. 4(a). Unlike in bulk crystals,[27] T_N in our $Mn_{3+x}Sn_{1-x}$ thin films is sensitive to compositional changes. Close to the stoichiometric point, T_N remains unchanged at around 390 K. However, as x increases, T_N drops significantly in a step-like manner, stabilizing at ~315 K for $x \geq 0.13$. This stabilization of T_N corresponds to the solubility limit of Mn in Mn_3Sn, as evidenced by structural characterization [Fig. 1(f)]. The observed reduction in T_N toward 300 K on increasing x qualitatively explains the roll down of the AHE amplitudes at 300 K for $x \geq 0.12$ [Fig. 3(c)]. The corresponding reduction in H_c is shown in Fig. S3 of the supplementary material.

In general, the reduction in T_N in thin films compared to the bulk value is often attributed to weakened magnetic exchange interactions, or surface and interface-related effects. In the case of Mn_3Sn, previous studies on bulk samples reported different values of T_N between the surface and bulk regions.[22] In our study, the primary effects may be related to a strain-induced lattice distortion caused by both the reduced dimensionality and epitaxial strain, since T_N in the studied films shows a clear correlation with the a lattice parameter, as depicted in Fig. 4(b). However, it must be acknowledged that a diffusion of atoms from adjacent layers within the stack cannot be ruled out.[49] The deposited layers are subjected to high-temperature annealing, which is essential to achieve the desired m-plane orientation of the films. Nevertheless, all layers are prepared under identical conditions in terms of stack design, thickness, and post-growth annealing conditions. As a result, any diffusion effects would systematically influence the absolute values of characteristic temperatures without altering the observed dependence on the layer composition or a.

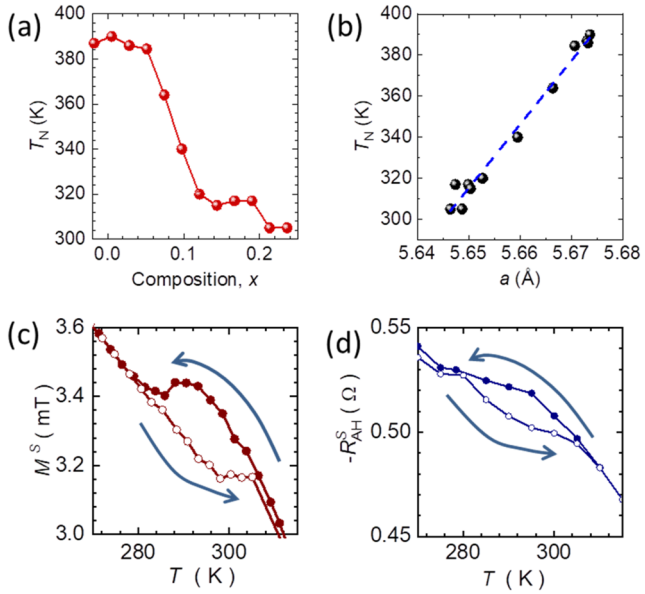

FIG. 4. $Mn_{3+x}Sn_{1-x}$ Néel temperature, T_N, dependence on (a) the composition, x, and (b) the a lattice parameter. (c) and (d) Thermal hysteresis of spontaneous magnetization, $M^S(T)$, and anomalous Hall resistance, $R^S_{AH}(T)$, respectively, around T_2 anomaly for $Mn_{3.10}Sn_{0.90}$.

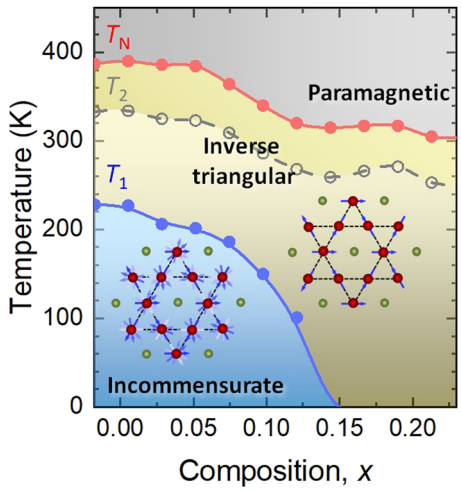

FIG. 5. Magnetic phase diagram of epitaxial $Mn_{3+x}Sn_{1-x}$ thin films. The symbols marking the boundaries between magnetic phases are established at a very weak external magnetic field, upon the positions of the characteristic points in the $dM^S(T)/dT$ derivatives, as illustrated in Fig. 2(c). The reddish bullets represent the Néel transition at T_N, while the blue ones mark the transition from the inverse triangular to an incommensurate spin arrangement at T_1. The open, gray symbols indicate the position of the magnetic anomaly, T_2, occurring consistently at 55 K below T_N in all the layers under study. The cartoons illustrate the spin arrangements in the inverse triangular and incommensurate structures of Mn_3Sn. The red bullets represent Mn atoms, and the arrows represent their spins. The greenish bullets represent Sn atoms.

D. Magnetic anomaly at T_2

The differentiation of the temperature-dependent data [Fig. 2(c)] clearly reveals the existence of a small magnetic anomaly between T_1 and T_N, labeled as T_2. This anomaly manifests as a distinct saddle point in either $M^S(T)$ or $R^S_{AH}(T)$, appearing roughly 55 K below T_N. Notably, this anomaly is ubiquitous, observed across all studied layers. Further investigation of T_2, as shown in Figs. 4(c) and 4(d), reveals thermal hysteresis in both M and R_{AH}. The presence of thermal hysteresis suggests a first order transition at T_2.

Similar anomalies in magnetization near the transition temperature are often observed in soft ferromagnetic materials and are attributed to the Hopkinson effect,[50] which occurs as a ferromagnet is heated toward its Curie temperature T_C due to increased domain wall mobility. However, in our study, the polarity of the AHE remains unchanged when crossing T_2. Therefore, rather than the domain pattern changes, it is more likely that only minor adjustments in the spin canting are involved. If so, these slightly different spin configurations must be separated by significant energy barriers to produce thermal hysteresis at such elevated temperatures.

We recognize that further experimental evidence is required to understand the origin of this anomaly and its potential role in Mn_3Sn-based devices. Nevertheless, the simultaneous appearance of such subtle features in both M and the AHE underscores the close relationship between the spin configuration details and the magnitude of the Berry curvature in Mn_3Sn.

E. $Mn_{3+x}Sn_{1-x}$ magnetic phase diagram

Our article concludes with Fig. 5, which depicts the magnetic phase diagram for epitaxial $Mn_{3+x}Sn_{1-x}$ films. We have established the position of the boundaries between three magnetic phases of $Mn_{3+x}Sn_{1-x}$ (paramagnetic, inverse triangular AFM, i.e., the commensurate with the lattice, and an incommensurate one) by determining the position of the characteristic points in $dM^S(T)/dT$ derivatives, as illustrated in Fig. 2(c). The extracted data show clear and smooth trends, indicating, in particular, that in epitaxial $Mn_{3+x}Sn_{x-1}$ films, the T_1 transition from IT-AFM to the incommensurate phase can be continuously tuned down until its complete suppression by increasing the Mn–Sn composition above approximately $x = 0.13$. Furthermore, it is observed that the T_2 anomaly trails T_N, consistently remaining ~55 K below it. We postulate, therefore, that the position of the T_2 anomaly can serve as a convenient indicator of T_N in layers with T_N exceeding 400 K, that is, above the typical temperature limit for most popular experimental setups.

IV. CONCLUSIONS

In summary, this study demonstrates that intrinsic alloying Mn_3Sn with Mn enables the extension of the temperature range, in which the unique topological and magnetic properties arising from the inverse triangular antiferromagnetic (IT-AFM) structure can be harnessed. The results clearly demonstrate that, within the framework of sputtering deposition, the T_1 temperature—marking the transition from the IT-AFM structure to an incommensurate spin configuration—can be precisely tuned by adjusting the Mn–Sn composition, ultimately leading to its complete suppression. This,

in turn, allows the strong anomalous Hall effect related to the magnetic octupole moment to persist down to the lowest temperatures. These findings open up new opportunities for applying the topological physics of Mn_3Sn at low temperatures, or could even lead to entirely new research directions.

Furthermore, we demonstrate that the Néel temperatures in our stacks of *m*-plane Mn_3Sn thin films are lower than the bulk values and that they decrease in accordance with the changes in *a* lattice parameter as the Mn content is increased. In addition, we report on the presence of a magnetic anomaly that appears consistently around 55 K below the Néel temperature and on the thermal hysteresis associated with it. In this context, well-planned temperature-dependent studies are essential for gaining deeper insights into the actual spin and electronic structures of this material family. Such investigations should extend into the high-temperature range (above 300 K), as the reduction in the Néel temperature, observed here, could play a critical role in experiments where Joule heating is unavoidable. In addition, the presence of thermal hysteresis—and associated energy barriers—warrants further exploration. The precise origin of this anomaly and its potential impact on device performance remain important questions for future research.

SUPPLEMENTARY MATERIAL

The supplementary material includes additional surface and compositional analyses (Sec. S.I., Fig. S1), as well as a discussion on the detrimental role of the magnetic response of MgO substrates in thin film magnetometry (Sec. S.II.), supported by Fig. S2. In addition, Sec. S.III presents the composition dependence of the coercive field H_c at 300 K, illustrated in Fig. S3.

ACKNOWLEDGMENTS

The authors thank Y. Nakano for the measurement of inductively coupled plasma mass spectrometry (ICP-MS) and R. Nomura for Hall bars fabrication. This work was partly supported by the TUMUG Support Program from Center for Diversity, Equity, and Inclusion, Tohoku University, JSPS KAKENHI (Grant Nos. 22K14558, 22KK0072, 24KJ0432, 24K22949, 24H02235, and 24H00039), JST-PRESTO (Grant No. JPMJPR24H6), JST-ASPIRE (Grant No. JPMJAP2322), MEXT Initiative to Establish Next-generation Novel Integrated Circuits Centers (X-NICS) (Grant No. JPJ011438), and RIEC Cooperative Research Projects.

AUTHOR DECLARATIONS

Conflict of Interest

The authors have no conflicts to disclose.

Author Contributions

K. Gas: Conceptualization (lead); Data curation (lead); Formal analysis (lead); Funding acquisition (equal); Investigation (lead); Methodology (lead); Visualization (lead); Writing – original draft (lead); Writing – review & editing (lead). **J.-Y. Yoon**: Funding acquisition (equal); Methodology (equal); Writing – review & editing (equal). **Y. Sato**: Funding acquisition (equal); Investigation (supporting); Writing – review & editing (equal). **H. Kubota**: Investigation (supporting); Writing – review & editing (equal). **P. Dłużewski**: Investigation (equal); Resources (equal); Writing – review & editing (equal). **S. Kret**: Investigation (equal); Resources (equal); Visualization (equal); Writing – review & editing (equal). **J. Z. Domagala**: Investigation (supporting); Resources (equal); Writing – review & editing (equal). **Y. K. Edathumkandy**: Investigation (supporting); Writing – review & editing (equal). **Y. Takeuchi**: Funding acquisition (equal); Writing – review & editing (equal). **S. Kanai**: Conceptualization (equal); Data curation (equal); Funding acquisition (equal); Writing – review & editing (equal). **H. Ohno**: Resources (equal); Writing – review & editing (equal). **M. Sawicki**: Conceptualization (equal); Data curation (equal); Formal analysis (equal); Investigation (equal); Methodology (equal); Resources (equal); Visualization (equal); Writing – original draft (lead); Writing – review & editing (lead). **S. Fukami**: Conceptualization (equal); Funding acquisition (lead); Resources (lead); Writing – review & editing (equal).

DATA AVAILABILITY

The data that support the findings of this study are available within the article and its supplementary material.

REFERENCES

[1] S. Nakatsuji, N. Kiyohara, and T. Higo, "Large anomalous Hall effect in a non-collinear antiferromagnet at room temperature," Nature **527**(7577), 212–215 (2015).
[2] A. K. Nayak, J. E. Fischer, Y. Sun, B. Yan, J. Karel, A. C. Komarek, C. Shekhar, N. Kumar, W. Schnelle, J. Kübler, C. Felser, and S. S. P. Parkin, "Large anomalous Hall effect driven by a nonvanishing Berry curvature in the noncolinear antiferromagnet Mn_3Ge," Sci. Adv. **2**(4), e1501870 (2016).
[3] L. Šmejkal, J. Sinova, and T. Jungwirth, "Beyond conventional ferromagnetism and antiferromagnetism: A phase with nonrelativistic spin and crystal rotation symmetry," Phys. Rev. X **12**(3), 031042 (2022).
[4] R. D. Gonzalez Betancourt, J. Zubáč, R. Gonzalez-Hernandez, K. Geishendorf, Z. Šobáň, G. Springholz, K. Olejník, L. Šmejkal, J. Sinova, T. Jungwirth, S. T. B. Goennenwein, A. Thomas, H. Reichlová, J. Železný, and D. Kriegner, "Spontaneous anomalous Hall effect arising from an unconventional compensated magnetic phase in a semiconductor," Phys. Rev. Lett. **130**(3), 036702 (2023).
[5] H. Reichlova, R. Lopes Seeger, R. González-Hernández, I. Kounta, R. Schlitz, D. Kriegner, P. Ritzinger, M. Lammel, M. Leiviskä, A. Birk Hellenes, K. Olejník, V. Petříček, P. Doležal, L. Horak, E. Schmoranzerova, A. Badura, S. Bertaina, A. Thomas, V. Baltz, L. Michez, J. Sinova, S. T. B. Goennenwein, T. Jungwirth, and L. Šmejkal, "Observation of a spontaneous anomalous Hall response in the Mn_5Si_3 d-wave altermagnet candidate," Nat. Commun. **15**(1), 4961 (2024).
[6] K. P. Kluczyk, K. Gas, M. J. Grzybowski, P. Skupiński, M. A. Borysiewicz, T. Fąs, J. Suffczyński, J. Z. Domagala, K. Grasza, A. Mycielski, M. Baj, K. H. Ahn, K. Výborný, M. Sawicki, and M. Gryglas-Borysiewicz, "Coexistence of anomalous Hall effect and weak magnetization in a nominally collinear antiferromagnet MnTe," Phys. Rev. B **110**(15), 155201 (2024).
[7] T. Nagamiya, "Triangular spin ordering in Mn_3Sn and Mn_3Ge," J. Phys. Soc. Jpn. **46**(3), 787–792 (1979).
[8] S. Tomiyoshi and Y. Yamaguchi, "Magnetic structure and weak ferromagnetism of Mn_3Sn studied by polarized neutron diffraction," J. Phys. Soc. Jpn. **51**(8), 2478–2486 (1982).
[9] J. W. Cable, N. Wakabayashi, and P. Radhakrishna, "A neutron study of the magnetic structure of Mn_3Sn," Solid State Commun. **88**(2), 161–166 (1993).
[10] M.-T. Suzuki, T. Koretsune, M. Ochi, and R. Arita, "Cluster multipole theory for anomalous Hall effect in antiferromagnets," Phys. Rev. B **95**(9), 094406 (2017).

[11]T. Nomoto and R. Arita, "Cluster multipole dynamics in noncollinear antiferromagnets," Phys. Rev. Res. **2**(1), 012045 (2020).
[12]K. Kuroda, T. Tomita, M.-T. Suzuki, C. Bareille, A. A. Nugroho, P. Goswami, M. Ochi, M. Ikhlas, M. Nakayama, S. Akebi, R. Noguchi, R. Ishii, N. Inami, K. Ono, H. Kumigashira, A. Varykhalov, T. Muro, T. Koretsune, R. Arita, S. Shin, T. Kondo, and S. Nakatsuji, "Evidence for magnetic Weyl fermions in a correlated metal," Nat. Mater. **16**(11), 1090–1095 (2017).
[13]H. Yang, Y. Sun, Y. Zhang, W.-J. Shi, S. S. P. Parkin, and B. Yan, "Topological Weyl semimetals in the chiral antiferromagnetic materials Mn_3Ge and Mn_3Sn," New J. Phys. **19**(1), 015008 (2017).
[14]M. Ikhlas, T. Tomita, T. Koretsune, M.-T. Suzuki, D. Nishio-Hamane, R. Arita, Y. Otani, and S. Nakatsuji, "Large anomalous Nernst effect at room temperature in a chiral antiferromagnet," Nat. Phys. **13**(11), 1085–1090 (2017).
[15]J. Han, T. Uchimura, Y. Araki, J.-Y. Yoon, Y. Takeuchi, Y. Yamane, S. Kanai, J. Ieda, H. Ohno, and S. Fukami, "Room-temperature flexible manipulation of the quantum-metric structure in a topological chiral antiferromagnet," Nat. Phys. **20**, 1110 (2024).
[16]X. Chen, T. Higo, K. Tanaka, T. Nomoto, H. Tsai, H. Idzuchi, M. Shiga, S. Sakamoto, R. Ando, H. Kosaki, T. Matsuo, D. Nishio-Hamane, R. Arita, S. Miwa, and S. Nakatsuji, "Octupole-driven magnetoresistance in an antiferromagnetic tunnel junction," Nature **613**(7944), 490–495 (2023).
[17]P. J. Brown, V. Nunez, F. Tasset, J. B. Forsyth, and P. Radhakrishna, "Determination of the magnetic structure of Mn_3Sn using generalized neutron polarization analysis," J. Phys.: Condens. Matter **2**(47), 9409 (1990).
[18]H. Tsai, T. Higo, K. Kondou, T. Nomoto, A. Sakai, A. Kobayashi, T. Nakano, K. Yakushiji, R. Arita, S. Miwa, Y. Otani, and S. Nakatsuji, "Electrical manipulation of a topological antiferromagnetic state," Nature **580**(7805), 608–613 (2020).
[19]Y. Takeuchi, Y. Yamane, J.-Y. Yoon, R. Itoh, B. Jinnai, S. Kanai, J. Ieda, S. Fukami, and H. Ohno, "Chiral-spin rotation of non-collinear antiferromagnet by spin–orbit torque," Nat. Mater. **20**(10), 1364–1370 (2021).
[20]T. Higo, K. Kondou, T. Nomoto, M. Shiga, S. Sakamoto, X. Chen, D. Nishio-Hamane, R. Arita, Y. Otani, S. Miwa, and S. Nakatsuji, "Perpendicular full switching of chiral antiferromagnetic order by current," Nature **607**(7919), 474–479 (2022).
[21]M.-W. Yoo, V. O. Lorenz, A. Hoffmann, and D. G. Cahill, "Thermal contribution to current-driven antiferromagnetic-order switching," APL Mater. **12**(8), 081107 (2024).
[22]A. L. Balk, N. H. Sung, S. M. Thomas, P. F. S. Rosa, R. D. McDonald, J. D. Thompson, E. D. Bauer, F. Ronning, and S. A. Crooker, "Comparing the anomalous Hall effect and the magneto-optical Kerr effect through antiferromagnetic phase transitions in Mn_3Sn," Appl. Phys. Lett. **114**(3), 032401 (2019).
[23]Y. Chen, J. Gaudet, G. G. Marcus, T. Nomoto, T. Chen, T. Tomita, M. Ikhlas, H. S. Suzuki, Y. Zhao, W. C. Chen, J. Strempfer, R. Arita, S. Nakatsuji, and C. Broholm, "Intertwined charge and spin density waves in a topological kagome material," Phys. Rev. Res. **6**(3), L032016 (2024).
[24]Y. Song, Y. Hao, S. Wang, J. Zhang, Q. Huang, X. Xing, and J. Chen, "Complicated magnetic structure and its strong correlation with the anomalous Hall effect in Mn_3Sn," Phys. Rev. B **101**(14), 144422 (2020).
[25]N. H. Sung, F. Ronning, J. D. Thompson, and E. D. Bauer, "Magnetic phase dependence of the anomalous Hall effect in Mn_3Sn single crystals," Appl. Phys. Lett. **112**(13), 132406 (2018).
[26]A. W. Overhauser, "Spin density waves in an electron gas," Phys. Rev. **128**(3), 1437–1452 (1962).
[27]E. Krén, J. Paitz, G. Zimmer, and É. Zsoldos, "Study of the magnetic phase transformation in the Mn_3Sn phase," Physica B+C **80**(1), 226–230 (1975).
[28]C. Singh, V. Singh, G. Pradhan, V. Srihari, H. K. Poswal, R. Nath, A. K. Nandy, and A. K. Nayak, "Pressure controlled trimerization for switching of anomalous Hall effect in triangular antiferromagnet Mn_3Sn," Phys. Rev. Res. **2**(4), 043366 (2020).
[29]K. Bhattacharya, A. K. Bharatwaj, C. Singh, R. Gupta, R. Khasanov, S. Kanungo, A. K. Nayak, and M. Majumder, "Hydrostatic and chemical pressure driven crossover from the commensurate to the incommensurate state of the Weyl semimetal $Mn_{3+x}Sn_{1-x}$," Phys. Rev. B **110**(9), 094432 (2024).
[30]K.-R. Jeon, B. K. Hazra, K. Cho, A. Chakraborty, J.-C. Jeon, H. Han, H. L. Meyerheim, T. Kontos, and S. S. P. Parkin, "Long-range supercurrents through a chiral non-collinear antiferromagnet in lateral Josephson junctions," Nat. Mater. **20**(10), 1358–1363 (2021).
[31]J. Yoon, Y. Takeuchi, R. Itoh, S. Kanai, S. Fukami, and H. Ohno, "Crystal orientation and anomalous Hall effect of sputter-deposited non-collinear antiferromagnetic Mn_3Sn thin films," Appl. Phys. Express **13**(1), 013001 (2019).
[32]Y. Takeuchi, H. Sepehri-Amin, S. Sugimoto, T. Hiroto, and S. Kasai, "Magnetic and magneto-transport properties of non-collinear antiferromagnetic Mn3Ge epitaxial films," APL Mater. **12**(7), 071110 (2024).
[33]M. Raju, R. Romero, D. Nishio-Hamane, R. Uesugi, M. Asakura, Z. Tagay, T. Higo, N. P. Armitage, C. Broholm, and S. Nakatsuji, "Anisotropic anomalous transport in the kagome-based topological antiferromagnetic Mn_3Ga epitaxial thin films," Phys. Rev. Mater. **8**(1), 014204 (2024).
[34]J.-Y. Yoon, Y. Takeuchi, S. DuttaGupta, Y. Yamane, S. Kanai, J. Ieda, H. Ohno, and S. Fukami, "Correlation of anomalous Hall effect with structural parameters and magnetic ordering in $Mn_{3+x}Sn_{1-x}$ thin films," AIP Adv. **11**(6), 065318 (2021).
[35]T. Uchimura, J.-Y. Yoon, Y. Sato, Y. Takeuchi, S. Kanai, R. Takechi, K. Kishi, Y. Yamane, S. DuttaGupta, J. Ieda, H. Ohno, and S. Fukami, "Observation of domain structure in non-collinear antiferromagnetic Mn_3Sn thin films by magneto-optical Kerr effect," Appl. Phys. Lett. **120**(17), 172405 (2022).
[36]M. Sawicki, W. Stefanowicz, and A. Ney, "Sensitive SQUID magnetometry for studying nanomagnetism," Semicond. Sci. Technol. **26**(6), 064006 (2011).
[37]K. Gas and M. Sawicki, "In situ compensation method for high-precision and high-sensitivity integral magnetometry," Meas. Sci. Technol. **30**(8), 085003 (2019).
[38]M. Khalid, A. Setzer, M. Ziese, P. Esquinazi, D. Spemann, A. Pöppl, and E. Goering, "Ubiquity of ferromagnetic signals in common diamagnetic oxide crystals," Phys. Rev. B **81**(21), 214414 (2010).
[39]L. Scheffler, K. Gas, S. Banik, M. Kamp, J. Knobel, H. Lin, C. Schumacher, C. Gould, M. Sawicki, J. Kleinlein, and L. W. Molenkamp, "Molecular beam epitaxy of the half-Heusler antiferromagnet CuMnSb," Phys. Rev. Mater. **4**(11), 114402 (2020).
[40]M. Wang, C. Andrews, S. Reimers, O. J. Amin, P. Wadley, R. P. Campion, S. F. Poole, J. Felton, K. W. Edmonds, B. L. Gallagher, A. W. Rushforth, O. Makarovsky, K. Gas, M. Sawicki, D. Kriegner, J. Zubáč, K. Olejník, V. Novák, T. Jungwirth, M. Shahrokhvand, U. Zeitler, S. S. Dhesi, and F. Maccherozzi, "Spin flop and crystalline anisotropic magnetoresistance in CuMnAs," Phys. Rev. B **101**(9), 094429 (2020).
[41]L. Scheffler, J. Werther, K. Gas, C. Schumacher, C. Gould, M. Sawicki, J. Kleinlein, and L. W. Molenkamp, "Bulk-like magnetic properties in MBE-grown unstrained, antiferromagnetic CuMnSb," Appl. Phys. Lett. **121**(1), 012401 (2022).
[42]A. Ciechan, P. Dłużewski, S. Kret, K. Gas, L. Scheffler, C. Gould, J. Kleinlein, M. Sawicki, L. W. Molenkamp, and P. Bogusławski, "Coexistence of antiferromagnetic cubic and ferromagnetic tetragonal polymorphs in epitaxial CuMnSb films," Phys. Rev. B **110**(1), 014436 (2024).
[43]G. J. Zimmer and E. Kren, "Investigation of the magnetic phase transformation in Mn_3Sn," AIP Conf. Proc. **5**(1), 513–516 (1972).
[44]M. Ikhlas, S. Dasgupta, F. Theuss, T. Higo, S. Kittaka, B. J. Ramshaw, O. Tchernyshyov, C. W. Hicks, and S. Nakatsuji, "Piezomagnetic switching of the anomalous Hall effect in an antiferromagnet at room temperature," Nat. Phys. **18**(9), 1086–1093 (2022).
[45]T. Ikeda, M. Tsunoda, M. Oogane, S. Oh, T. Morita, and Y. Ando, "Improvement of large anomalous Hall effect in polycrystalline antiferromagnetic Mn_{3+x} Sn thin films," IEEE Trans. Magn. **55**(7), 1–4 (2019).
[46]W. H. Meiklejohn and C. P. Bean, "New magnetic anisotropy," Phys. Rev. **102**(5), 1413–1414 (1956).
[47]X. F. Zhou, X. Z. Chen, Y. F. You, L. Y. Liao, H. Bai, R. Q. Zhang, Y. J. Zhou, H. Q. Wu, C. Song, and F. Pan, "Exchange bias in antiferromagnetic Mn_3Sn monolayer films," Phys. Rev. Appl. **14**(5), 054037 (2020).
[48]M. Zhao, W. Guo, X. Wu, L. Ma, P. Song, G. Li, C. Zhen, D. Zhao, and D. Hou, "Zero-field-cooling exchange bias up to room temperature in the strained kagome antiferromagnet $Mn_{3.1}Sn_{0.9}$," Mater. Horiz. **10**, 4597 (2023).
[49]J. Hayakawa, S. Ikeda, Y. M. Lee, F. Matsukura, and H. Ohno, "Effect of high annealing temperature on giant tunnel magnetoresistance ratio of CoFeB/MgO/CoFeB magnetic tunnel junctions," Appl. Phys. Lett. **89**(23), 232510 (2006).
[50]J. Hopkinson, "I. Magnetic properties of alloys of Nickel and iron," Proc. R. Soc. London **48**(292–295), 1–13 (1891).